LOW SPEED EXPERIMENTAL AND NUMERICAL INVESTIGATIONS ON UNCONVENIONAL CONTROL CONCEPTS FOR AGILE AND HIGHLY SWEPT AIRCRAFT CONFIGURATIONS

M. Paul*, M. Rütten, M. Rein
DLR, Institute for Aerodynamics and Flow Technology
Bunsenstraße 10, 37073 Göttingen, Germany

Abstract

Various unconventional control concepts are considered for placement on the SACCON aircraft. The scaled-down DLR-F17E model is used as the numerical and experimental vehicle. The first category of control concepts is motivated by the desire to improve aircraft stability and control while maintaining a clean signature from ground-based sensors. The second category is motivated by the promise of smooth surface deformations eliminating control surface gaps. Each concept is studied at Re = 762,000 and U_∞ = 52m/s using the DLR TAU code with the intention of verifying results through a test campaign in the low speed 1 Meter Tunnel, Göttingen. Only a limited number of control concepts were built and tested in the wind tunnel, and their results are compared with the CFD results to highlight differences in the methods. The CFD results for each concept are presented and their merits are discussed.

1. INTRODUCTION

The use of delta and lambda wing configurations has increased in recent years as the reliance on Unmanned Combat Air Vehicles (UCAV) has surged. The tailless lambda wing configuration is desirable for its stealth characteristics and natural aerodynamic efficiency, but poses significant stability and control challenges. Future UCAVs will need to achieve stealth performance as well as high maneuverability, two factors which directly oppose each other due to the stealth penalty of traditional control surfaces.

The German Aerospace Center (DLR) has conducted many numerical and experimental studies on the generic lambda wing SACCON (Stability And Control CONfiguration) with a leading edge sweep angle of 53°[1]. These have focused on using traditional trailing edge control surfaces to create the desired forces and moments. These techniques were then applied to the DLR-F19 or DLR-F17E wind tunnel models for low and high speed testing. Instead, this study explores new ideas for control surface design and placement for eventual testing on the DLR-F17E model. The suffix “E” denotes the presence of an optional engine intake which remained covered during these tests. For a discussion on traditional control surfaces on the DLR-F19 model, see Huber et. al[2], Rein et. al[3], or Vicroy et. al[4].

The flow over the SACCON aircraft is highly vortical at medium to high angles of attack, resulting in non-linear aerodynamics[5-7]. As a result, control surface effectiveness is not easily predicted and therefore lends itself to numerical simulation. The numerical investigations are completed with the DLR flow solver TAU running steady Reynolds Averaged Navier-Stokes (RANS) simulations.

There are two main categories of control systems considered in this paper. The first concept uses control surfaces on the upper surface of the aircraft to keep the view from ground based sensors unchanged. The second concept uses smooth deformations of the wingtips to eliminate control surface gaps. The CFD results from each concept are presented and compared against experimental results where available.

2. EXPERIMENTAL MODEL

2.1. DLR-F17E Configuration

The DLR-F17E is a tailless lambda-wing configuration with a leading edge sweep of 53° and varying leading edge radius. The wing leading edge changes from sharp at the apex, to round through the middle section, and again sharp at the wing tip. The wings include a 5° washout. The model has been scaled down from the original SACCON configuration at 1:20.5 in order to fit into transonic wind tunnels[8]. The model is shown in Figure 1 with a clean upper surface.

* Michael Paul is an employee of the Directed Energy Directorate, Air Force Research Laboratory in Albuquerque, New Mexico. He is working at DLR as a member of the Engineer and Scientist Exchange Program. The work presented here is entirely funded and coordinated by DLR.

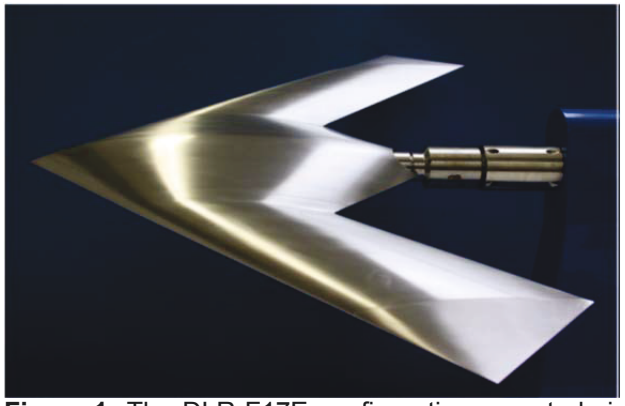

Figure 1: The DLR-F17E configuration mounted via rear sting on a display stand.

The DLR-F17E has a modular design which allows quick changes to the configuration. The wing leading edges, wing tips, and trailing edges can all be quickly changed to study the effects of various control surfaces. In addition, there are cutouts in the upper surface plate of the fuselage which resemble an engine duct. For these tests, the base configuration has a clean surface without the engine duct or trailing edge flaps.

The force and moment coefficients are shown in this paper. The force coefficients are calculated using the free stream dynamic pressure, q_∞, and the planform area, S_{ref}. The moment coefficients also require a reference length. The roll and yaw moment coefficients use the wing half span and the pitch moment coefficient uses the mean aerodynamic chord. The planform area, S_{ref} = 0.1173m^2, accounts for a small cutout for the rear sting. The wing half span is s = 0.30m and the mean aerodynamic chord is l_μ = 0.2342m. The neutral point, x_{N25} = 0.212m, is the Moment Reference Point (MRP). The location of the MRP and the model dimensions are shown in Figure 2. Note that other values have typically been used for the SACCON's pitching moment reference length and for the location of the MRP[2,4,9].

2.2. Control Concepts

The focus of this study was to examine the effects of unconventional control methods using quick-reaction panel deflections and smooth surface deformations to improve flight stability and controllability. To this end, there are a number of concepts discussed below. Only the base configuration and the fuselage spoilers were tested in the wind tunnel because the other concepts were not built in time for testing. All of the concepts presented here were tested numerically.

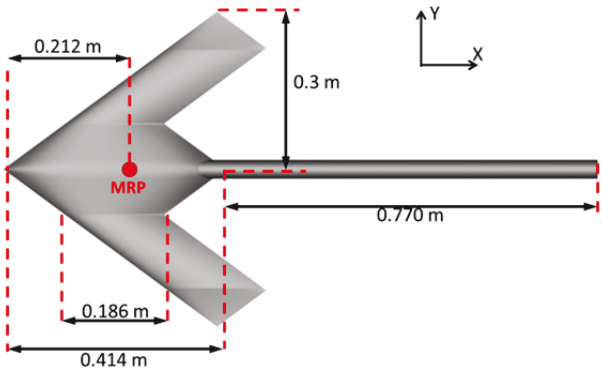

Figure 2: A top view of the DLR-F17E showing the wing halfspan, the location of the Moment Reference Point and other reference lengths.

2.2.1. Fuselage Spoilers

There are two large spoilers located at the aft end of the central fuselage section. The panels as shown in Figure 3 are deflected 50° trailing edge up, with the hinge line along the surface contour in the y-direction. The spoilers' trailing edge angles at zero deflection match the fuselage's trailing edge angles. The spoilers could be deflected in unison to create a pitch moment or individually to create a roll moment. When only one fuselage spoiler is present, it is mounted on the left side with a clean surface on the right. In the results, the single fuselage spoiler concept is labelled, "1x F. Spoiler", while the concept with both fuselage spoilers is labelled, "2x F. Spoilers".

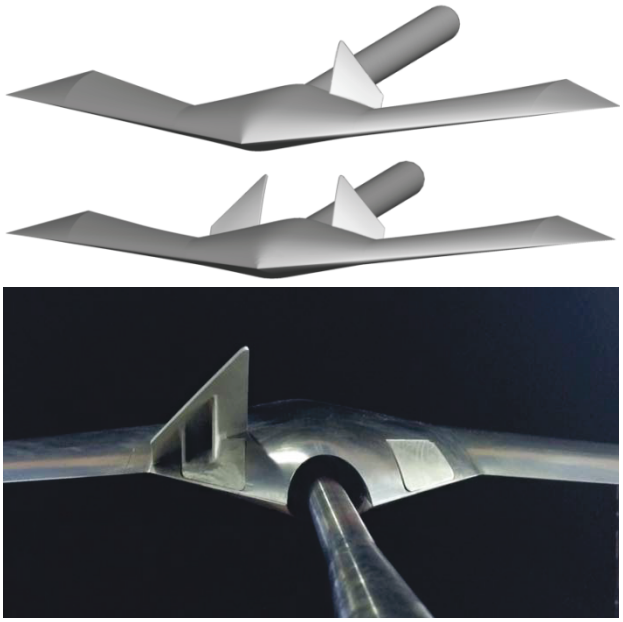

Figure 3: The model with aft fuselage spoilers deflected 50°. The rear supports are visible at the bottom for the wind tunnel model.

2.2.2. Wing Devices

A fence and a spoiler are considered on the upper surface near the leading edge of the wing to have a greater impact on the flow. The fence is placed parallel to the leading edge of the left wing. It is 6.2mm tall and 100mm wide, taking 27% of the wing halfspan due to the 53° leading edge sweep. The front face is protruded in the z-direction with the lower edge extended aft for attachment to the experimental model. The fence location and shape are seen in Figure 4. The fence is limited in its spanwise placement by the wingtips due to a desire to prevent control devices from crossing over seams in the model. On an operational aircraft, a quick-reaction actuator would allow for rapid correction while maintaining a small imperfection on the upper surface of the wing.

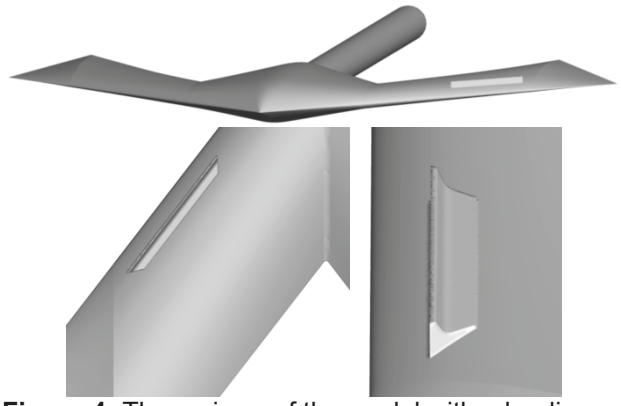

Figure 4: Three views of the model with a leading edge fence. The lower right picture shows the extended lower surface for attaching the fence to the experimental model.

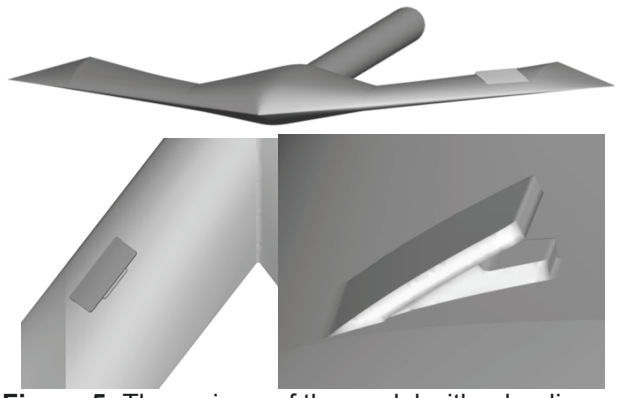

Figure 5: Three views of the model with a leading edge spoiler. The lower right picture shows the extended lower surface for attaching the spoiler to the experimental model.

To prevent vertical surfaces during actuation, the spoiler is placed in the same area with matching vertical displacement. As a comparison, the spoiler location and geometry are shown in Figure 5. The spoiler length is limited to 20% of the wing chord and the width-to-length ratio is 2.5 due to the desire to place a traditional spoiler near the leading edge. As a result, the width of the spoiler is 57mm, shorter than the 100mm leading edge fence. The upper surface of the spoiler maintains wing curvature while rotated up 20°. There is a plate under the spoiler which acts as an attachment surface to the model during wind tunnel testing.

2.2.3. Wingtips

There are two twisted wingtip configurations, both of which use the same smooth deformation. The wings of the clean configuration already have a 5° washout (trailing edge up). For this concept, the wingtips are rotated an additional 7.5° about the y-axis while the remaining wing sections are unchanged. The wingtips can be rotated in the same or opposite directions to cause a primary pitch or roll moment, respectively. As shown in Figure 6, the right wingtip is rotated leading edge down in both configurations for a total effect of 12.5° washout. The left wingtip is rotated either leading edge up or down resulting in 12.5° washout or 2.5° wash-in, respectively.

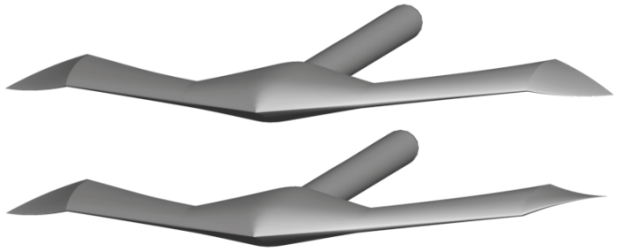

Figure 6: The model with smooth wingtip twisting. The wingtips can be twisted symmetrically (top) to create a primary pitch moment or asymmetrically (bottom) to create a primary roll moment.

2.2.4. Drooped Tips

The wingtips are smoothly rotated 30° downward about axes parallel to the x-axis to improve the yaw static stability derivative, C_{n_β}. These do not rotate about the y-axis like the wingtips presented above and therefore offer no yaw command. The drooped tips in Figure 7 provide only a corrective yawing moment in the onset of sideslip. The downward rotation maintains yaw stability when the flow over the wing is separated.

Figure 7: The model with 30° drooped tips.

3. EXPERIMENTAL SETUP

The DLR-F17E model was tested in the 1-Meter Tunnel (1MG) of the German Aerospace Center (DLR), Institute of Aerodynamics and Flow Technology. The 1MG is an atmospheric, closed circuit facility that can be operated with an open or closed test section. This study used the open test section with a 1.5m length and a rectangular nozzle

measuring 1.0m x 0.74m. The 1:5.2 contraction ratio yields a maximum velocity of 64m/s. At 52m/s, the maximum velocity for these tests, the tunnel turbulence is between 0.14 – 0.32%[10]. A side view of the tunnel is shown in Figure 8. The model was installed via a rear sting with integrated pitch and yaw control. During these tests, the pitch was varied from 0° to 30° in one degree increments. The model remained at zero yaw throughout the tests. The flow velocity was varied from 10m/s to 52m/s, but only the data at 52m/s are presented in this paper.

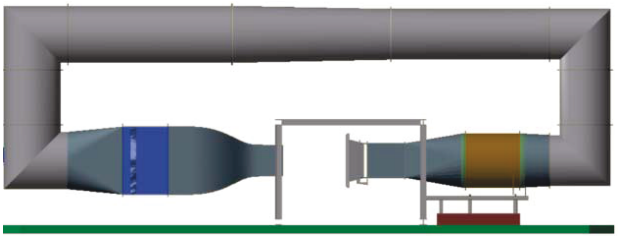

Figure 8: Side view of the 1MG showing the open test section.

The forces and moments were measured via a 6-component strain gauge. The flow conditions were derived from pressure and temperature measurements in the tunnel.

4. NUMERICAL SETUP

The numerical simulations were setup for direct comparisons with the experimental results. To this end, the DLR-F17E geometry and flow conditions match those used in the tunnel.

4.1. Grid Generation

The DLR-F17E model with rear sting and a clean upper surface has been used for the numerical investigations. The control devices either mount flush with the aircraft geometry or are attached to the upper surface, as shown in Figure 4 and Figure 5. The grids were created using the commercial tool Centaur. The different geometries each use the same grid generation inputs, but their individual features cause some variation in the final grids. To fully resolve the boundary layer, especially on the leading edge, the initial wall spacing is 0.005mm with 20 pseudo structured layers. As a result, the maximum y^+ of 1.6 occurs at the sharp leading edge of the wingtips. The upper and lower surfaces and the majority of the leading edge are limited to $y^+ < 1.0$. Figure 9 shows the y^+ contours on the upper surface of the model. The farfield is defined as a sphere with radius 50 times the wing halfspan. All other surfaces are defined as viscous, no-slip walls. The resulting grid for the clean configuration has 1.9 million grid points and 6.3 million total elements.

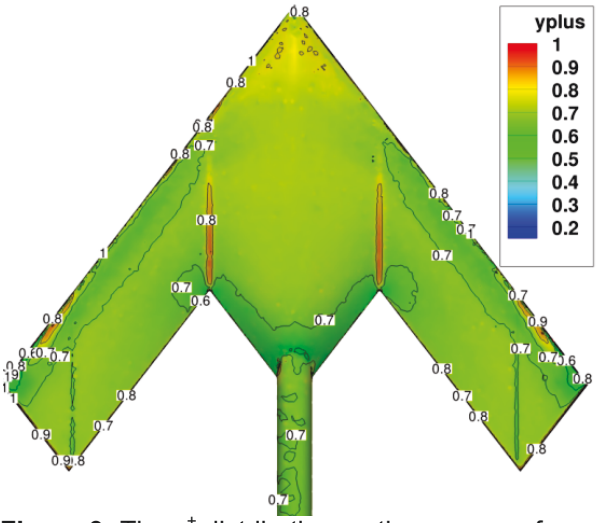

Figure 9: The y^+ distribution on the upper surface of the DLR-F17E model at U_∞ = 52m/s, Re = 762,000.

4.2. Flow Solution

The numerical investigations are completed with the DLR flow solver TAU running steady RANS simulations. The code has a second order spatial and temporal discretization. The Spalart-Allmaras negative turbulence model was used due to its proven accuracy with this model[11].

For direct comparison, the farfield conditions were set to match the experimental conditions. The farfield velocity was set to 52m/s at a temperature of 302K and a pressure of 100,145Pa. The resulting Reynolds number is 762,000. Due to the number of configurations, an angle of attack sweep was not carried out in one degree increments. Instead, the simulations were completed at α = [0°, 10°, 13°, 15°, 17°, 20°], even though vortex breakdown begins to invalidate the steady assumption around 17°[11].

5. RESULTS

Only the base configuration and the fuselage spoiler configurations were tested in the wind tunnel. The other configurations were not built in time and will be tested at a later date. The CFD results are presented for all configurations to show the impacts of each control concept.

5.1. Experimental Results vs CFD

The lift coefficient (C_L), drag coefficient (C_D) and pitching moment coefficient (C_m) are compared to evaluate the agreement between the experimental and CFD results because these coefficients vary primarily with angle of attack. The side force coefficient (C_Y), rolling moment coefficient (C_l) and yawing moment coefficient (C_n) are not considered here because they vary primarily with angle of sideslip and wind tunnel data was not taken at non-zero angles of sideslip. The specifics of each model are briefly addressed.

5.1.1. Clean Configuration

The clean configuration was first tested to provide a baseline of comparison for the other configurations. As seen in Figure 10, the CFD sufficiently models C_D but there are small discrepancies in C_L. However, there are large errors in modelling C_m. Jirásek et. al have recorded the difficulty in modelling C_m with a number of different CFD solvers[12]. Turbulent simulations and a higher quality grid would be required to accurately predict C_m. The difference at $\alpha = 0°$ is small, but the slope throughout the alpha sweep is too negative.

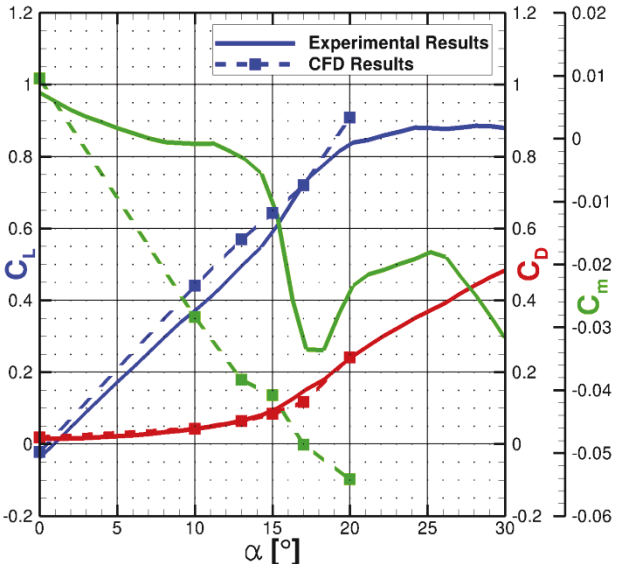

Figure 10: C_L, C_D, and C_m comparison between CFD and experimental results for the clean, baseline configuration.

5.1.2. Single Fuselage Spoiler

The CFD for the single fuselage spoiler matches C_D between 0° and 20°, but with small errors in C_L. The errors in C_m are consistent with the errors with the clean model. It is worth noting that while the slope of C_m in Figure 11 is off between 0° and 15°, it does nose down sharply between 15° and 20°, just as in the experimental results.

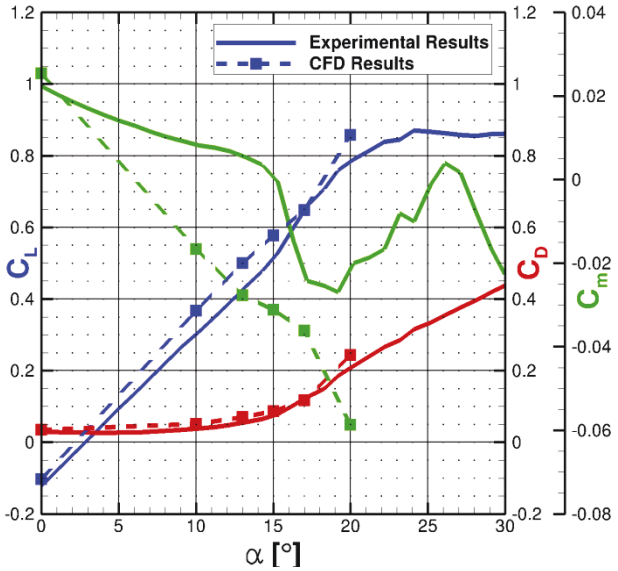

Figure 11: C_L, C_D, and C_m comparison between CFD and experimental results for the single fuselage spoiler.

5.1.3. Both Fuselage Spoilers

The trends discussed above are seen with both spoilers activated, but with increased magnitude. The CFD continues to model C_D acurately between 0° and 20°, with small errors in C_L. Once again, the CFD fails to capture the proper slope of C_m, but does show the drop off between 15° and 20°.

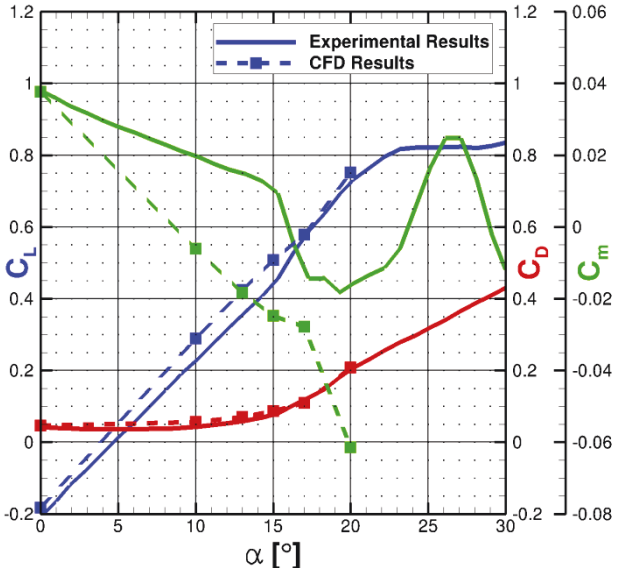

Figure 12: C_L, C_D, and C_m comparison between CFD and experimental results for both fuselage spoilers.

5.2. CFD Results For All Control Concepts

The CFD results for all force and moment coefficients are compared for each control concept. To identify the individual effects quickly, only the effects of the new control device are shown. For

any given coefficient, i, the results from the clean DLR-F17E are subtracted from those of the new models.

$$\Delta C_i = C_{i_{controls}} - C_{i_{clean}}$$

The results for each configuration are shown in Figure 13.

5.2.1. Single Fuselage Spoiler

The single fuselage spoiler causes a ΔC_L = -0.08 at α = 0° with a small increase in C_D, despite the large frontal surface area of the deployed spoiler. The large loss in lift is limited to the left side of the fuselage, causing a negative roll moment, although at 20° the ΔC_l is less strong. There is also a large drop off in ΔC_m at higher angles of attack, with 0.16 reduction of ΔC_m from 17° to 20°. Due to the location of the spoiler with respect to the x-axis and the desire for yaw control, the fuselage spoilers were made quite large. However, despite the large surface area, the maximum ΔC_n = 0.005.

5.2.2. Both Fuselage Spoilers

The configuration with both fuselage spoilers is symmetric, so the ΔC_Y, ΔC_l, and ΔC_n are negligible, of $O(10^{-4})$. The other impacts are similar in nature to those of the single fuselage spoiler, but with greater magnitude. The spoilers cause a significant loss in lift across the range of angle of attack, such that $\Delta C_L \approx$ -0.15. There is an initial drag increase, with ΔC_D = 0.28 at α = 0°, but it steadily decreases, eventually showing a drag reduction at α > 17. In the case of low speed vehicles, drag production is a combination of skin friction, induced drag, and pressure drag. The skin friction difference between the clean configuration and the two spoiler concept is not enough to cause this difference. As the flow separates further upstream and the body of the aircraft shields the spoilers, the pressure difference behind the spoilers is of less importance. The main factor remaining is the loss in lift production by the rest of the aircraft, which causes ΔC_D to steadily decline. Such a large influence on the flow field above the aft fuselage also causes a significant increase in ΔC_m. With both spoilers, the drop off of ΔC_m between 17° and 20° is nearly double that of the single fuselage spoiler.

5.2.3. Leading edge fence

The leading edge fence creates a flat surface which directly obstructs the oncoming flow and affects the flow field over much of the left wing. Since the leading edge fence is angled at 53°, the force on the fence is seen in both the ΔC_D and ΔC_Y plots, with both having similar profiles and magnitudes. The sudden obstruction over the left wing creates a proportional yaw moment. The maximum yaw effect is ΔC_n = -0.009 at 13°. The fence has almost no impact on ΔC_l until α = 15°. At this point, the upstream vertical edge of the fence generates a sufficiently strong vortex to energize the flow behind the fence. This localized effect accounts for the increase in ΔC_L and ΔC_l until α = 20°. The nonlinear aerodynamic effects are clearly visible at α = 20°, where there is a sudden improment in ΔC_D, and in the direction of ΔC_Y and ΔC_n. A higher density of CFD test points would be needed to resolve the progression between 17° and 20°, but such a rapid change in the coefficients proves the difficulty in predicting performance for these configurations.

5.2.4. Leading edge spoiler

The leading edge spoiler, with its similar location and matching displacement to the leading edge fence, causes a similar response. The ΔC_D, ΔC_l, and ΔC_m plots each have the trends and magnitudes as the leading edge fence values, although the ΔC_D for the leading edge spoiler has a slower onset. The differences between the two control concepts in side force and yaw moment are nearly identical at non-zero angles of attack. In general, though, the leading edge spoiler effects are smaller, though this could be explained by the 43% shorter width. A wider spoiler would add drag and side force between 0° and 15° angles of attack, at which point the flow is separated over the spoiler. These additional forces, and the resulting yawing moment, would bring the leading edge spoiler results closer to the fence's.

5.2.5. Asymmetric Wingtip Twist

The asymmetrically twisted wingtips create the greatest roll moment of any of the considered control concepts. The roll moment improvement is steady throughout the angle of attack range and has a maximum value of ΔC_l = 0.016. The deformations have only a small impact on ΔC_L, ΔC_D or ΔC_m as the left and right wingtips largely cancel each other out. This asymmetric configuration has the greatest side force when α > 15°. It also has the greatest impact on yawing moment at α = 0°, when ΔC_n = 0.004. The ΔC_n steadily decreases until α = 15° as the two wingtips stall separately.

5.2.6. Symmetric Wingtip Twist

The symmetrically twisted wingtips create a primary pitch moment by adding an additional 7.5° washout. As a result, $\Delta C_m \approx$ 0.01 until α = 20°, when the wingtips have stalled. By further washing-out the wingtips, however, there is a $\Delta C_L \approx$ -0.015 between 0° and 20°. Drag initially increases, due to the increased frontal area of the rotated wingtips, but steadily decreases with increased angle of attack as the wingtips stall later than the clean configuration.

5.2.7. Drooped Tips

The drooped tips' main purpose is to provide a corrective yawing moment at non-zero angles of sideslip, but they noticeably affect C_L and C_m between 0° and 20° angles of attack. Due to the downward rotation of a section of the wing lifting

surface, C_L is reduced at each angle of attack, with the maximum change of ΔC_L = -0.035 at α = 15°. This is the only configuration with a positive slope in the ΔC_m plot, also reaching its maximum value of ΔC_m = 0.021 at α = 15°.

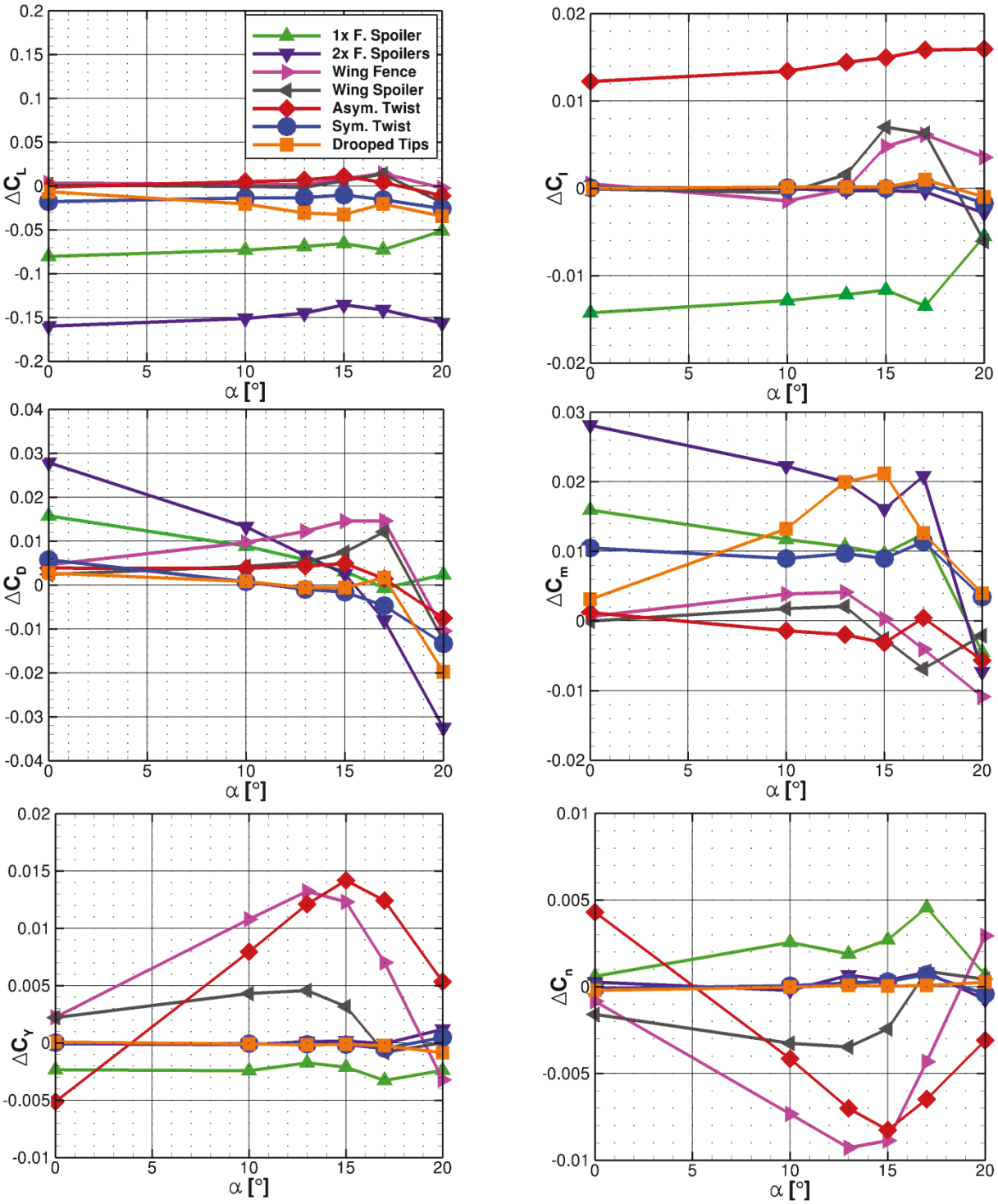

Figure 13: The change in the force and moment coefficients caused by each new control concept on the DLR-F17E, Re = 762,000.

5.3. Yaw Control

The yaw stability of an aircraft has great importance. The yawing moment coefficients are shown in Figure 14 for each model between -5° and 5° angles of sideslip. The first thing to note is the C_n produced by the asymmetric wingtip twist model. Given a range of small beta, this has the largest effect. Twisting the wingtips in the opposite direction would have the same magnitude response but of opposite sign.

This could have potential for yaw control if the other forces and moments can be accounted for in the control logic because the primary effect created by this wingtip twist is a roll moment. Perhaps the more useful result is the effect of the drooped tips. This deformation produces the greatest C_{n_β} and has an additional benefit due to its symmetry. The asymmetric wingtip twist model has a greater magnitude effect on C_n, but it would have to rotate its wingtips back and forth to correct sideslip from each side. The drooped tips configuration corrects sideslip from either side with only one deformation.

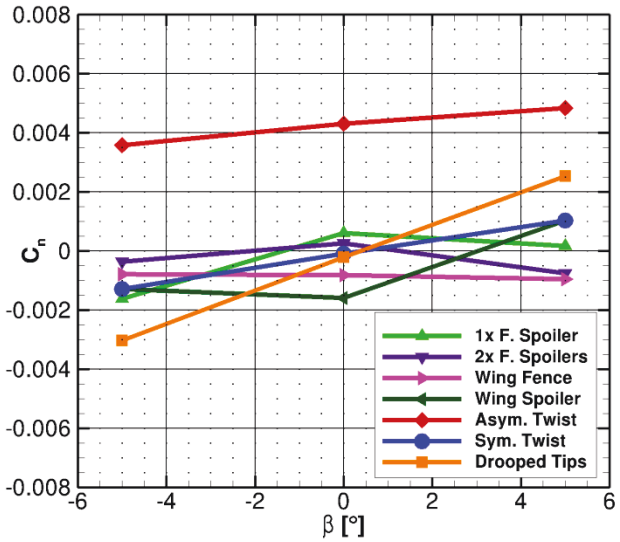

Figure 14: The CFD yawing moment coefficient results for each model at α = 0°, β = [-5°, 0°, 5°], Re = 762,000.

6. CONCLUSIONS

The tailless lambda wing configuration is a highly desirable aircraft configuration due to its natural stealth benefits and aerodynamic efficiency. However, it poses several problems to stability and control, particularly in yaw. Several new control concepts were developed to limit the aircraft signature from ground based sensors and to take advantage of smoothly deforming structures. A CFD campaign tested each concept at 52m/s at a range of angles of attack. A wind tunnel campaign set out to verify the CFD results, but only a limited number of configurations were built in time for testing.

When looking at the coefficients which vary with angle of attack, the wind tunnel and CFD results yield similar results for each the three configurations tested in the 1MG. The pitch moment coefficient continues to be a challenge in properly modelling. The wind tunnel results closely match previous data, implying that the error here lies with the CFD calculation. The results at α = 0° have little error, but a higher quality grid and running turbulent simulations would be required to accurately predict C_m for these models when α > 10°.

The fuselage spoiler configurations were designed to create strong roll, pitch and yaw moments. The single fuselage spoiler does create a yaw response, but the roll moment has a greater response. The double fuselage spoiler configuration creates a large lift and drag penalty and probably would not be useful outside of being an airbrake.

The leading edge fence and leading edge spoiler were designed to look similar and were placed in a similar location. The fence provides a smaller disturbance on the wing surface while the spoiler does not present a flat frontal area. The main difference in the results between these models can likely be explained by their length differences. The leading edge could serve as an adequate yaw command device as its effect on the other coefficients is small. A spoiler could achieve similar levels of performance as the fence, but questions need to be answered regarding the aspect ratio and size of the spoiler, as it requires a larger wing surface area.

The two twisted wingtip configurations offer an alternative to traditional flapped control surfaces and avoid gaps altogether. Despite the limited surface area, the asymmetric twist concept achieves a $\Delta C_l \approx 0.01$ and the symmetric twist concept achieves a $\Delta C_m \approx 0.01$ against the clean DLR-F17E configuration. Although the asymmetric twist model can achieve yaw control, other control surfaces would need to counteract the primary rolling moment.

While the drooped tips pay a small price in lift, they are a simple and effective way to achieve yaw stability at small angles of sideslip. These do not command yaw, so crosswind landings and coordinated turns are still unresolved problems.

Additional testing will occur in October 2015 at subsonic and transonic Mach numbers. Each configuration discussed here will be tested, allowing a more complete comparison between CFD and experimental results.

7. REFERENCES

[1] Schütte, A., Hummel, D., Hitzel, S., “Flow Physics Analyses of a Generic Unmanned Combat Aerial Vehicle Configuration,” J. Aircraft 49, 1638 – 1651, 2012.

[2] Huber, K. C., Schütte, A., Rein, M., and Löser, T., "Experimental aerodynamic assessment and evaluation of an agile highly swept aircraft configuration", Deutscher Luft- und Raumfahrtkongress, Rostock, 22. - 24. September 2015.

[3] Rein M., Irving, J. P., Rigby, G., and Birch, T. J., “High Speed Static Experimental Investigations to Estimate Control Device Effectiveness and S&C Capabilities,” AIAA 2014-2004, 2014.

[4] Vicroy, D. D., Huber, K. C., Schütte, A., Rein, M., Irving, J. P., Rigby, G., Löser. T., Hübner, A.-R., and Birch, T. J., Experimental Investigations of a Generic 53° Swept UCAV Configuration with Controls, to be submitted to J. Aircraft, 2015.

[5] Hummel, D. “Effects of boundary layer formation on the vortical flow above slender delta wings”, RTO AVT Symposium on “Enhancement of NATO Military Flight Vehicle Performance by Management of Interacting Boundary Layer Transition and Separation”, Prague, Czech Republic, 4-8 Oct 2004, Meeting Proceedings RTO-MP-AVT-111, 30-1 to 30-22, 2004.

[6] Kandil, O.A., Chuang, H.A. “Computation of Vortex-Dominated Flow for a Delta Wing Undergoing Pitching Oscillation", AIAA Journal vol. 28 no. 9 Sep. 1990 pp 1589-1595, 1990.

[7] Spaid, F.W., Hakkinen, R.J. “On the Boundary Layer Displacement Effect Near the Trailing Edge of an Aft-Loaded Airfoil", Journal of Applied Mathematics and Physics (ZAMP), vol. 28, 1977.

[8] Rein M., “Measurements of aerodynamic forces and moments on the DLR-F17 model in low- and high-speed flows,” DLR Report No. IB 224–2011 A61, 2011.

[9] Huber, K., Schütte, A., Rein, M., “Numerical Investigation of the Aerodynamic Properties of a Flying Wing Configuration.”, AIAA 2012-3325, 2012.

[10] Wolf, C., priv. com., 2015.

[11] Rütten, M., Saalfeld, B., Rein, M., Künemund, J., Saalfeld, S., “Numerical Flow Investigation of Morphing Leading Edges for the Enhancement of Maneuverability of Unmanned Combat Air Vehicles”, AIAA 2012-3326, 2012.

[12] Jirásek, A., Cummings, R., Schütte, A., Huber, K., “The NATO STO AVT-201 Task Group on Extended Assessment of Stability and Control Prediction Methods for NATO Air Vehicles: Summary”, AIAA 2014-2394, 2014.